

PRODUCTION OF MO AND RU ISOTOPES IN NEUTRINO-DRIVEN WINDS: IMPLICATIONS FOR SOLAR ABUNDANCES AND PRESOLAR GRAINS

J. BLISS

Institut für Kernphysik, Technische Universität Darmstadt, Schlossgartenstr. 2, Darmstadt 64289, Germany

A. ARCONES

Institut für Kernphysik, Technische Universität Darmstadt, Schlossgartenstr. 2, Darmstadt 64289, Germany
GSI Helmholtzzentrum für Schwerionenforschung GmbH, Planckstr. 1, Darmstadt 64291, Germany

Y.-Z. QIAN

School of Physics and Astronomy, University of Minnesota, Minneapolis, MN 55455, USA
Tsung-Dao Lee Institute, Shanghai 200240, China

Draft version April 12, 2018

ABSTRACT

The origin of the so-called p -isotopes $^{92,94}\text{Mo}$ and $^{96,98}\text{Ru}$ in the solar system remains a mystery as several astrophysical scenarios fail to account for them. In addition, data on presolar silicon carbide grains of type X (SiC X) exhibit peculiar Mo patterns, especially for $^{95,97}\text{Mo}$. We examine production of Mo and Ru isotopes in neutrino-driven winds associated with core-collapse supernovae (CCSNe) over a wide range of conditions. We find that proton-rich winds can make dominant contributions to the solar abundance of ^{98}Ru , significant contributions to those of ^{96}Ru ($\lesssim 40\%$) and ^{92}Mo ($\lesssim 27\%$), and relatively minor contributions to that of ^{94}Mo ($\lesssim 14\%$). In contrast, neutron-rich winds make negligible contributions to the solar abundances of $^{92,94}\text{Mo}$ and cannot produce $^{96,98}\text{Ru}$. However, we show that some neutron-rich winds can account for the peculiar Mo patterns in SiC X grains. Our results can be generalized if conditions similar to those studied here are also obtained for other types of ejecta in either CCSNe or neutron star mergers.

1. INTRODUCTION

The isotopic abundances of the solar system obtained from meteoritic data (see e.g., Lodders 2003) played a crucial role in establishing the framework of the basic processes of nucleosynthesis that gave rise to these abundances in particular and were responsible for the chemical evolution of the universe in general. For elements heavier than Fe, it is well known that the major sources for their solar abundances are the slow (s) and rapid (r) neutron-capture processes (Burbidge et al. 1957; Cameron 1957). In a number of cases, the most proton-rich isotopes of an element cannot be made by either of these processes and must be attributed to the so-called p -process (see e.g., Meyer 1994; Arnould & Goriely 2003). There have been both observational and theoretical studies that strongly support low-mass ($\sim 1.5\text{--}3 M_{\odot}$) stars during the asymptotic giant branch (AGB) stage of their evolution as the site for the main s -process producing Sr and heavier elements (see e.g., Käppeler et al. 2011). It is also well known that massive ($> 10 M_{\odot}$) stars during their pre-supernova evolution can produce nuclei up to ^{88}Sr through the weak s -process starting with the Fe in their birth material (see e.g., Raiteri et al. 1993; Pignatari et al. 2010). The p -process is usually associated with (γ, n) reactions on the preexisting nuclei as the shock propagates through the outer shells of a massive star during its supernova explosion (see Pignatari

et al. 2016 for a review). A kilonova powered by the decay of newly-synthesized r -process nuclei in a binary neutron star merger was observed recently (e.g., Smartt et al. 2017; Kasen et al. 2017). This observation demonstrates that mergers of two neutron stars or a neutron star and a black hole are important sites for the r -process (see e.g., Freiburghaus et al. 1999b; Goriely et al. 2011; Korobkin et al. 2012). Other sites (see e.g., Woosley & Hoffman 1992; Banerjee et al. 2011; Nishimura et al. 2015) associated with core-collapse supernovae (CCSNe) from massive stars have also been proposed and may play an important role in r -process enrichment at the earliest epochs (see e.g., Qian & Wasserburg 2007; Qian 2014; Hansen et al. 2014).

In connection with modeling CCSNe (see e.g., Janka 2012 for a review), new mechanisms for producing the elements from Zn to Ag with mass numbers $A \sim 64\text{--}110$ have been discovered (Woosley & Hoffman 1992; Hoffman et al. 1996; Pruet et al. 2006; Fröhlich et al. 2006). These are associated with neutrino-driven winds from the proto-neutron star created in a CCSN. Depending on the electron fraction, entropy, and expansion time scale (see e.g., Qian & Woosley 1996), major production of some of the above elements occurs in the wind (see e.g., Witt et al. 1994; Hoffman et al. 1997; Arcones & Montes 2011; Arcones & Bliss 2014). In these processes, (n, γ) , (n, p) , (p, γ) , (α, γ) , (α, n) , (α, p) and their inverse reactions are all important (Woosley & Hoffman 1992; Bliss et al. 2017), in contrast to the dominance of neutron capture in both the s - and r -processes. For proton-rich winds, $\bar{\nu}_e + p \rightarrow n + e^+$ can provide neutrons to break

through the bottleneck nuclei with slow β -decay by efficient (n, p) reactions. This νp -process (Pruet et al. 2006; Fröhlich et al. 2006; Wanaajo 2006) can produce nuclei up to $A \sim 110$ and perhaps even further for the most favorable conditions.

As described above, a wide range of nuclei with $A \sim 64$ –110 conventionally assigned to the s -, r -, and p -processes can be produced in neutrino-driven winds through very different mechanisms. The corresponding yield patterns are sensitive to the conditions in the wind (see e.g., Arcones & Bliss 2014; Bliss et al. 2018) and usually distinct from the solar abundance pattern in this region. The isotopes $^{92,94}\text{Mo}$ and $^{96,98}\text{Ru}$ are commonly taken to be produced by the p -process only, but p -process models have difficulty accounting for their solar abundances (see e.g., Meyer 1994; Arnould & Goriely 2003). In this paper, we explore a wide range of wind conditions to study the production of Mo and Ru isotopes and the implications for the solar abundances of $^{92,94}\text{Mo}$ and $^{96,98}\text{Ru}$. Further, in light of the peculiar Mo patterns, especially for $^{95,97}\text{Mo}$, and the associated anomalies in Zr found in presolar silicon carbide grains of type X (SiC X; Pellin et al. 1999, 2006), we also discuss possible nucleosynthetic contributions to these grains from neutrino-driven winds. Our results can be generalized if conditions similar to those explored here are also obtained for other types of ejecta in either CCSNe or neutron star mergers. Consequently, our study is complementary to post-processing studies based on specific simulations of these events.

2. PARAMETRIC MODELS OF NEUTRINO-DRIVEN WINDS

Nucleosynthesis in an expanding mass element starting from high temperature and density depends on the entropy S , expansion time scale τ , and electron fraction Y_e (Qian & Woosley 1996; Hoffman et al. 1997; Meyer & Brown 1997; Freiburghaus et al. 1999a; Otsuki et al. 2000; Thompson et al. 2001). So the main features of such nucleosynthesis can be captured by parametric studies. Typically the evolution of the temperature T with time t is taken as some function $T(t)$ characterized by the time scale τ [e.g., $T(t) \propto \exp(-t/\tau)$]. As the entropy S is mainly a function of T and the density ρ (e.g., $S \propto T^3/\rho$ for radiation-dominated conditions), the time evolution of ρ can be obtained from $T(t)$ by assuming conservation of S . For an initial temperature $T(0) \sim 10$ GK, the nuclei present (predominantly free neutrons and protons) are in nuclear statistical equilibrium (NSE), so the initial composition can be determined by the NSE equations along with mass and charge conservation. Because the matter of concern is neutral, the sum of all nuclear charge can be specified by the electron fraction Y_e . Thus, for a set of S , τ , and Y_e , the corresponding nucleosynthesis can be followed with a reaction network.

Compared to the generic parametric studies described above, the studies presented here include additional ingredients of realistic astrophysical environments with intense neutrino fluxes. Specifically, we use as the baseline models the trajectories of three mass elements in the neutrino-driven wind from the proto-neutron star in the CCSN model M1511rl of Arcones et al. (2007). This explosion model has an efficient neutrino transport scheme that allows to study the evolution of the wind for various progenitors in one and two dimensions (Arcones

et al. 2007; Arcones & Janka 2011). However, simplifications in the treatment of neutrinos and the proto-neutron star lead to uncertainties in the explosion and the subsequent neutrino-driven wind. In view of these uncertainties, while we adopt the time evolution of the temperature $T(t)$ and the radius $r(t)$ for three trajectories of wind mass elements ejected at time post core bounce $t_{\text{pb}} = 2, 5, \text{ and } 8$ s, respectively, we vary the entropy and the electron fraction. For a trajectory with an original entropy S_0 and the corresponding density evolution $\rho_0(t)$, we change the entropy to $S = (0.5\text{--}1.5)S_0$ and obtain the new density evolution $\rho(t) = \rho_0(t)S_0/S$ assuming $S \propto T^3/\rho$. In addition, we vary the initial Y_e over the range $Y_e(0) = 0.45\text{--}0.62$ and follow the subsequent evolution of Y_e by including ν_e and $\bar{\nu}_e$ absorption on free neutrons and protons, respectively. We assume that the ν_e ($\bar{\nu}_e$) spectrum is Fermi-Dirac with temperature T_{ν_e} ($T_{\bar{\nu}_e}$) and zero chemical potential. Further, we fix $L_{\nu_e} = 2 \times 10^{51}$ ergs/s and calculate $L_{\bar{\nu}_e} = L_{\nu_e}T_{\bar{\nu}_e}/T_{\nu_e}$ assuming equal ν_e and $\bar{\nu}_e$ number fluxes. For neutron-rich (proton-rich) winds, we fix $T_{\nu_e} = 4$ MeV ($T_{\bar{\nu}_e} = 4$ MeV) and choose $T_{\bar{\nu}_e}$ (T_{ν_e}) to match the $Y_e(0)$. The ν_e and $\bar{\nu}_e$ fluxes experienced by a mass element decrease with time as $r(t)^{-2}$. The parametric models for the neutrino-driven wind described above should represent rather well both the variation of conditions with the time of ejection from the proto-neutron star in an individual CCSN and the variation among CCSNe from different progenitors.

In Fig. 1a, we present the baseline temperature and density evolution for the three chosen trajectories. The baseline entropy is $S_0 = 67, 78, \text{ and } 85$ in units of Boltzmann constant per nucleon (k_B/nuc) for the wind mass element ejected at $t_{\text{pb}} = 2, 5, \text{ and } 8$ s, respectively. The kinks in $T(t)$ and $\rho_0(t)$ are caused by the reverse shock when the wind runs into the material ejected at earlier times. Clearly, this type of time evolution cannot be simply parametrized by a single time scale τ . As discussed below, the reverse shock at wind termination plays a crucial role in the νp -process (see e.g., Wanaajo et al. 2011; Arcones et al. 2012).

To calculate the nucleosynthesis, we use the same reaction network as in Fröhlich et al. (2006), which includes 4053 nuclei corresponding to the elements from H to Hf. The reaction rates are taken from JINA ReaclibV1.0 (Reaclib 2013), which is a compilation of theoretical rates from Rauscher & Thielemann (2000) and experimental rates from Angulo et al. (1999). The theoretical weak reaction rates in Fröhlich et al. (2006) are supplemented with experimental β -decay rates (NuDat2 2013) when available. The calculations start at $T(0) \sim 10$ GK, for which the composition is calculated from NSE for the specific $Y_e(0)$. The subsequent evolution of the nuclear composition and Y_e is calculated using the full network that includes ν_e and $\bar{\nu}_e$ absorption on free neutrons and protons, respectively (Fröhlich et al. 2006). As described above, we always adjust the ν_e and $\bar{\nu}_e$ luminosities and spectra so that they are consistent with the specified $Y_e(0)$ (Arcones & Bliss 2014). The evolution of the radius $r(t)$ used to calculate that of the ν_e and $\bar{\nu}_e$ fluxes is shown in Fig. 1b.

In Figs. 1c and 1d, we illustrate the nucleosynthesis for our baseline models assuming $Y_e(0) = 0.45$ (neutron-rich) and 0.60 (proton-rich), respectively. It can be seen

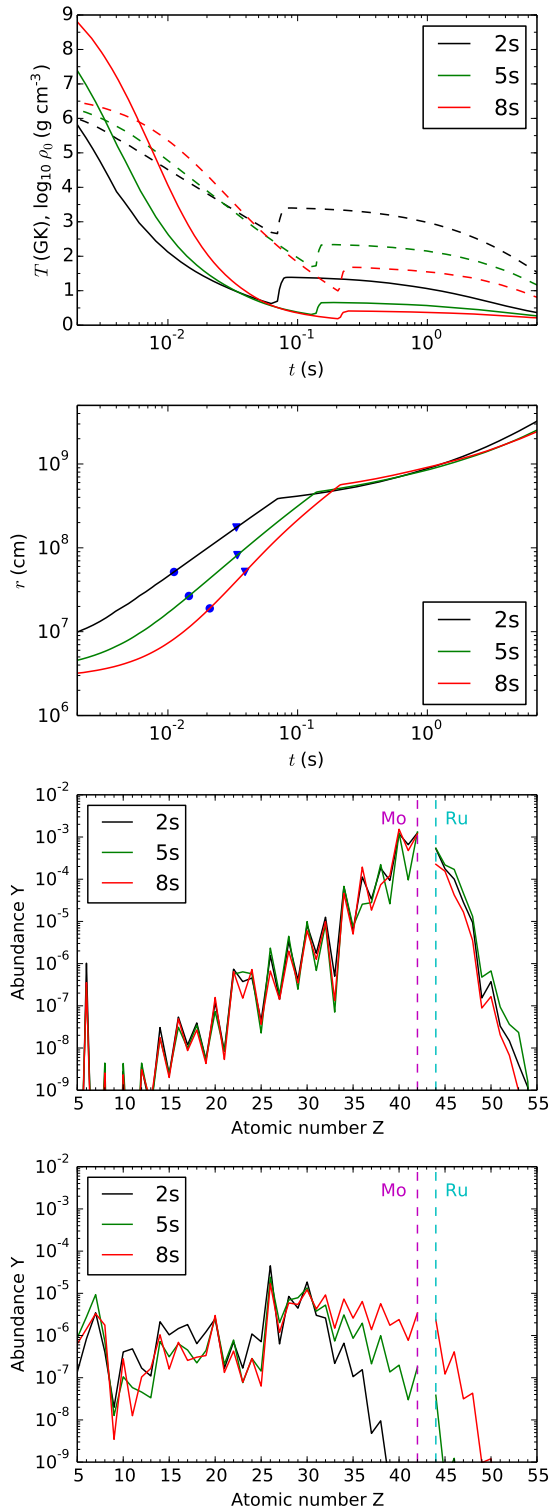


FIG. 1.— Baseline models for nucleosynthesis. (a) Time evolution of T/GK (solid curves) and $\log(\rho/\text{g cm}^{-3})$ (dashed curves) for trajectories of wind mass elements ejected at $t_{\text{pb}} = 2$ (black curves), 5 (green curves), and 8 s (red curves), respectively. (b) Time evolution of the radius r for each trajectory. The region of $T = 2$ to 1 GK important to the νp -process is indicated as that between the solid circle and triangle. (c) The final elemental (number) abundances for each trajectory assuming $Y_e(0) = 0.45$ (neutron-rich). (d) Same as (c), but for $Y_e(0) = 0.60$ (proton-rich).

that the variations of $T(t)$ and S_0 among the three tra-

jectories have a minor impact on the final abundances for neutron-rich conditions when the same $Y_e(0)$ is used. However, the situation is markedly different for proton-rich conditions, where increasingly heavier nuclei are produced for the wind mass elements ejected at later times. This is because the expansion affects the νp -process in such conditions through the determination of both the number ratio of protons to seed nuclei and the $\bar{\nu}_e$ flux at the onset of the process. Specifically, the expansion time scale for $T \sim 6$ to 3 GK sets the number ratio of protons to seed nuclei at the onset of the νp -process. In addition, this time scale also determines the radius of the mass element, and hence the $\bar{\nu}_e$ flux it receives, at this onset. Finally, the combination of this $\bar{\nu}_e$ flux and the expansion time scale for $T \sim 2$ to 1 GK determines the extent of neutron production by $\bar{\nu}_e$ absorption on protons during the νp -process. Clearly, a sufficient neutron abundance is required to overcome the bottlenecks on the path to heavier nuclei via (n, p) reactions. The slowing down of the mass element near the wind termination helps to fulfill this requirement. The trajectory ejected at $t_{\text{pb}} = 2$ s has the fastest initial expansion and the mass element is already at a large radius at the onset of the νp -process (see Fig. 1b). Therefore, for this trajectory $\bar{\nu}_e$ absorption on protons is strongly reduced during the νp -process even with the slowing down of the expansion near the wind termination. In contrast, the overall expansion for the trajectory ejected at $t_{\text{pb}} = 8$ s is slower so that the νp -process becomes much more efficient and reaches significantly heavier nuclei.

In the following discussion, we will focus on the trajectory ejected at $t_{\text{pb}} = 8$ s. Pertinent results for the other two trajectories are also presented. As described above, our study is parametric in that we adopt fixed evolution of temperature $T(t)$ and radius $r(t)$ for a wind trajectory while varying S and $Y_e(0)$ to obtain a range of $\rho(t)$ and $Y_e(t)$, respectively. We note that only accurate modeling of a specific astrophysical environment can yield a self-consistent set of $T(t)$, $\rho(t)$, and $Y_e(t)$. In the case of the neutrino-driven wind, this would require accurate neutrino transport in the proto-neutron star and accurate simulation of the CCSN explosion (Arcones & Thielemann 2013; Arcones & Bliss 2014). While our parametric approach can only serve as approximation to the rigorous astrophysical models, it captures the salient features of such models that are important to heavy-element nucleosynthesis. Further, it is efficient for surveying a wide range of possibilities. The results from our parametric models should provide good guidance in finding the conditions for producing Mo and Ru isotopes of interest.

3. RESULTS ON MO AND RU ISOTOPES

We are interested in the conditions under which various Mo and Ru isotopes can be made in environments similar to the neutrino-driven wind. In conventional terms, the seven stable isotopes of Mo (Ru) fall into four categories: (1) $^{92,94}\text{Mo}$ ($^{96,98}\text{Ru}$) as the p -only nuclei, (2) ^{96}Mo (^{100}Ru) as the s -only nuclide, (3) $^{95,97,98}\text{Mo}$ ($^{99,101,102}\text{Ru}$) as the mixed nuclei with contributions from the s - and r -processes, and (4) ^{100}Mo (^{104}Ru) as the r -only nuclide. As mentioned in the introduction, all these isotopes can be produced in the wind by processes that differ from the conventional p -, s -, and r -processes. How-

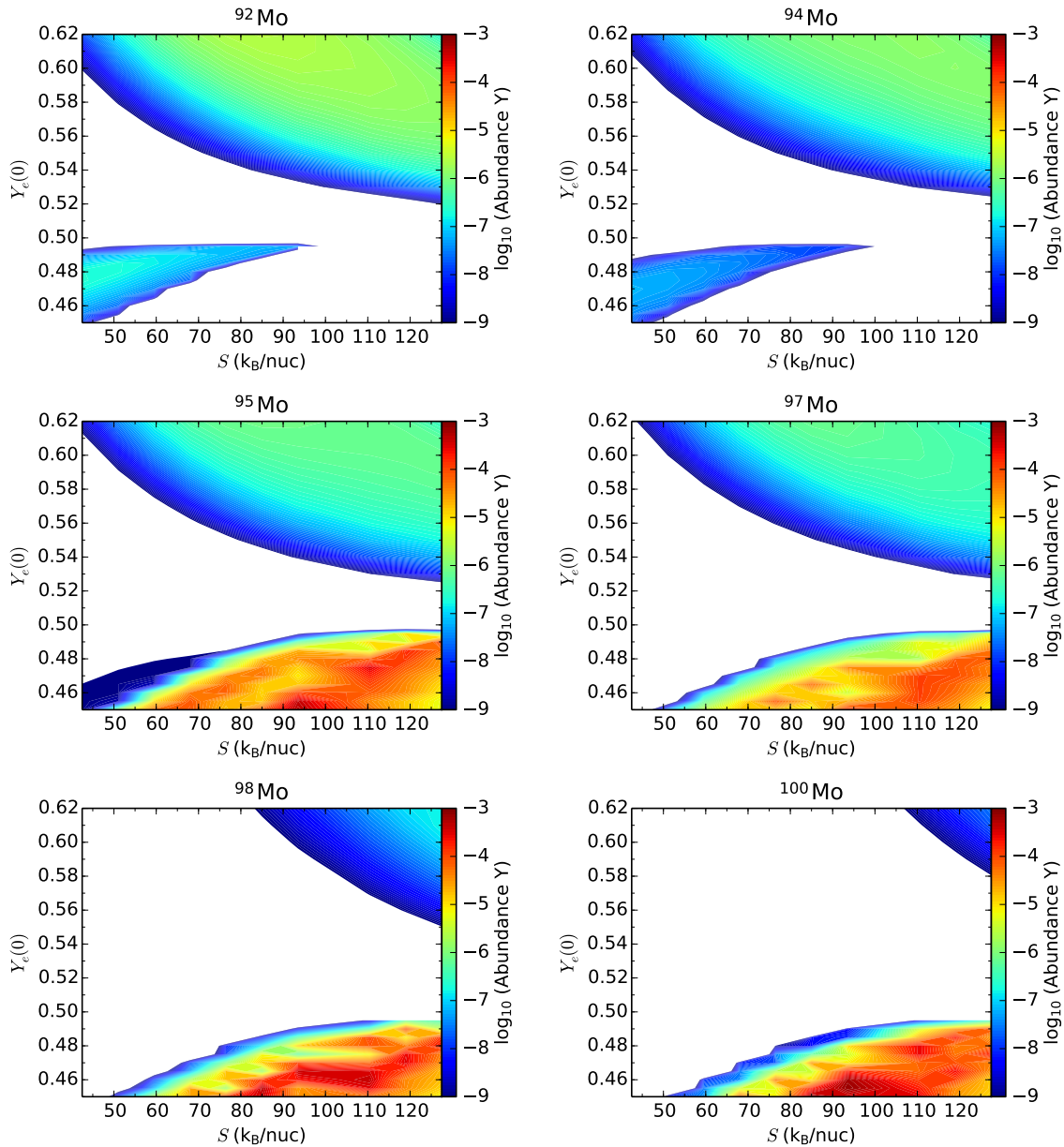


FIG. 2.— Color-coded contours illustrate the abundances (on a logarithmic scale) of the indicated isotope produced by the trajectory ejected at $t_{\text{pb}} = 8$ s for different $Y_e(0)$ and S . Abundances smaller than 10^{-9} are shown in white.

ever, for convenience, we will refer to these isotopes using the above conventional category labels.

Based on the trajectory ejected at $t_{\text{pb}} = 8$ s, we present in Fig. 2 (3) the abundances of various Mo (Ru) isotopes as functions of S and $Y_e(0)$. Figure 2 shows that both the p -only nuclei $^{92,94}\text{Mo}$ can be produced in slightly neutron-rich [$Y_e(0) < 0.5$] or proton-rich [$Y_e(0) > 0.5$] winds for a significant range of S . In contrast, the p -only nuclei $^{96,98}\text{Ru}$ can be produced only in proton-rich winds but not in neutron-rich winds (see Fig. 3).

Two distinct processes are responsible for producing $^{92,94}\text{Mo}$ in neutron- and proton-rich conditions, respectively. Neither of these processes are dominated by neutron capture. To reach $^{92,94}\text{Mo}$ in neutron-rich conditions, the nucleosynthesis path has to move along the valley of stability. If the neutron abundance is too large, the path goes farther to the neutron-rich side and production

of $^{92,94}\text{Mo}$ is blocked by $^{92,94}\text{Zr}$, respectively. Therefore, production of $^{92,94}\text{Mo}$ requires that very few neutrons be present at freeze-out of charged-particle reactions with the composition dominated by α -particles and seed nuclei (see also Hoffman et al. 1996; Wanajo 2006; Farouqi et al. 2009). In addition to neutron capture, reactions involving light charged-particles (e.g., protons and α -particles) play important roles in producing the seed nuclei including $^{92,94}\text{Mo}$. Larger abundances of these two isotopes are obtained for smaller S , which favors a smaller number ratio of neutrons to the seed nuclei.

In proton-rich conditions, $^{92,94}\text{Mo}$ are produced by the νp -process, where (p, γ) and (n, p) reactions play key roles in driving the flow towards heavy nuclei. The (p, γ) reactions clearly depend on the proton abundance, and so do the (n, p) reactions with $\bar{\nu}_e + p \rightarrow n + e^+$ providing the neutrons. Because a larger $Y_e(0)$ and a higher S fa-

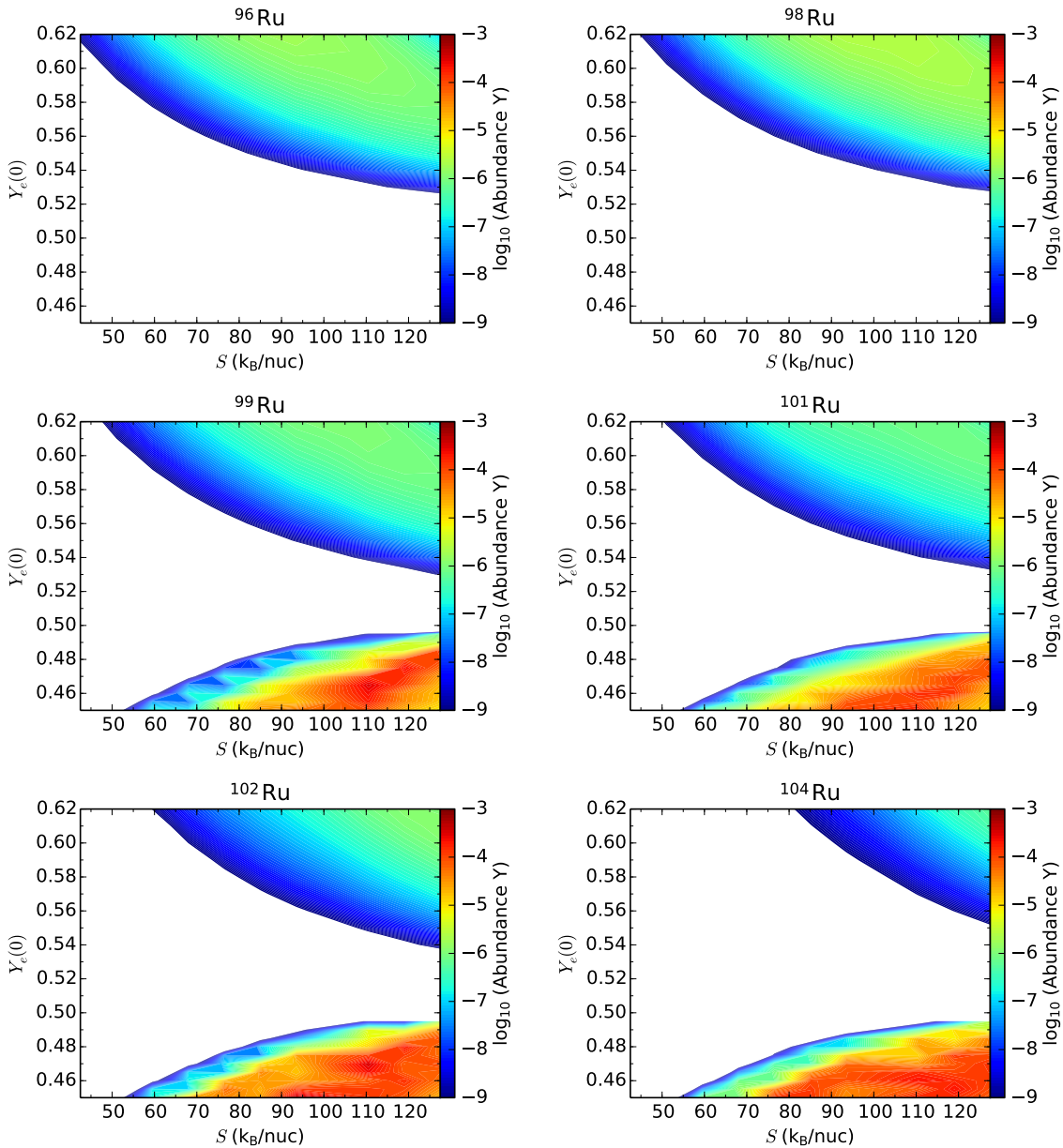


FIG. 3.— Same as Fig. 2, but for Ru isotopes.

vor a higher proton abundance, the νp -process produces more $^{92,94}\text{Mo}$ with increasing $Y_e(0)$ and S initially (Pruet et al. 2006). However, when the number ratio of protons to the seed nuclei reaches a threshold, the abundances of $^{92,94}\text{Mo}$ start to decrease as the flow moves towards heavier nuclei.

The abundances of $^{92,94}\text{Mo}$ are rather low in neutron-rich conditions (see Fig. 2). Because the nucleosynthesis path towards the p -only nuclei $^{96,98}\text{Ru}$ passes through $^{92,94}\text{Mo}$, no significant amounts of $^{96,98}\text{Ru}$ can be synthesized in neutron-rich conditions. In contrast, $^{96,98}\text{Ru}$ can be produced in proton-rich conditions similarly to $^{92,94}\text{Mo}$ (see Fig. 3).

The mixed nuclei $^{95,97,98}\text{Mo}$ and $^{99,101,102}\text{Ru}$, as well as the r -only nuclei ^{100}Mo and ^{104}Ru , are much more abundant in neutron-rich conditions (see Figs. 2 and 3). Their production is due to neutron capture and generally increases for lower $Y_e(0)$ and higher S , which favor a

higher ratio of neutrons to the seed nuclei. For typical neutron-rich conditions investigated here, the neutron-capture process stays close to the valley of stability on the neutron-rich side. Once the neutrons are consumed, β -decays populate $^{95,97,98,100}\text{Mo}$ and $^{99,101,102,104}\text{Ru}$. For conditions giving rise to a high ratio of neutrons to the seed nuclei, the nucleosynthesis path moves further away from stability and towards heavier nuclei, which leads to a decrease in production of Mo and Ru isotopes.

The s -only nuclei ^{96}Mo and ^{100}Ru can be synthesized only in proton-rich winds by late (n, γ) reactions (see Arcones et al. 2012; Fröhlich et al. 2006; Wanajo 2006). For this production channel to occur, a sufficient number of neutrons need to be available at the end of the νp -process. In any case, relative to the solar pattern of Mo (Ru) isotopes, the production of ^{96}Mo (^{100}Ru) is always much less significant than that of $^{92,94}\text{Mo}$ ($^{96,98}\text{Ru}$) for the conditions explored here (see e.g., Fig. 7).

3.1. Solar abundances of $^{92,94}\text{Mo}$ and $^{96,98}\text{Ru}$

In order for an astrophysical environment to be a major source for the solar abundance of an isotope ${}^i\text{E}$, a necessary condition is that this isotope must have a production factor $P({}^i\text{E})$ close to the maximum production factor P_{max} among all isotopes made in the same environment. The production factor $P({}^i\text{E})$ is defined as

$$P({}^i\text{E}) \equiv X({}^i\text{E})/X_{\odot}({}^i\text{E}), \quad (1)$$

where $X({}^i\text{E})$ and $X_{\odot}({}^i\text{E})$ are the mass fraction of the isotope ${}^i\text{E}$ produced in a model and observed in the solar system, respectively. The ratios $P({}^i\text{E})/P_{\text{max}}$ for $^{92,94}\text{Mo}$ and $^{96,98}\text{Ru}$ produced by the trajectory ejected at $t_{\text{pb}} = 8$ s are shown as color-coded contours for different S and $Y_e(0)$ in Fig. 4.

It can be seen from Fig. 4 that only ^{98}Ru can be produced with the maximum production factor in the wind. In fact, while $P(^{98}\text{Ru})/P_{\text{max}} \sim 1$ is reached at $S \sim 128$ k_{B}/nuc and $Y_e(0) \sim 0.61$, major production of ^{98}Ru occurs for a substantial range of conditions, e.g., $S \sim 80\text{--}128$ k_{B}/nuc for $Y_e(0) \sim 0.6$ or $Y_e(0) \sim 0.56\text{--}0.62$ for $S \sim 110$ k_{B}/nuc . In contrast, the highest value of $P({}^i\text{E})/P_{\text{max}}$ is ~ 0.4 [at $S \sim 77$ k_{B}/nuc , $Y_e(0) \sim 0.61$] for ^{96}Ru , ~ 0.27 [at $S \sim 111$ k_{B}/nuc , $Y_e(0) \sim 0.56$] for ^{92}Mo , and ~ 0.14 [at $S \sim 111$ k_{B}/nuc , $Y_e(0) \sim 0.56$] for ^{94}Mo . These results suggest that proton-rich winds can make dominant contributions to the solar abundance of ^{98}Ru , significant contributions to those of ^{96}Ru ($\lesssim 40\%$) and ^{92}Mo ($\lesssim 27\%$), and relatively minor contributions to that of ^{94}Mo ($\lesssim 14\%$). Figure 4 also shows that neutron-rich winds make negligible contributions to the solar abundances of $^{92,94}\text{Mo}$ and cannot produce any significant amounts of $^{96,98}\text{Ru}$.

The above results strongly suggest that sources other than the neutrino-driven wind, e.g., Type Ia supernovae (see Travaglio et al. 2014 for a recent study), are required to account for the solar abundances of $^{92,94}\text{Mo}$ and ^{96}Ru . Results for the trajectories ejected at $t_{\text{pb}} = 2$ and 5 s also support this conclusion (see Figs. 5 and 6). While proton-rich winds can make dominant contributions to the solar abundance of ^{98}Ru , the exact contribution from this source can be determined only when contributions from other sources are established.

We emphasize that in considering potential contributions from a source to the solar abundances of $^{92,94}\text{Mo}$ and $^{96,98}\text{Ru}$, the associated $P({}^i\text{E})/P_{\text{max}}$ values are a critical test. The production ratio of $^{92,94}\text{Mo}$ ($^{96,98}\text{Ru}$) relative to the solar value is secondary in that it is important only when the production factors for both isotopes are close to P_{max} . Because only ^{98}Ru can have $P(^{98}\text{Ru})/P_{\text{max}} \sim 1$ in the wind, explanation of the ratios $(^{92}\text{Mo}/^{94}\text{Mo})_{\odot} = 1.60$ and $(^{96}\text{Ru}/^{98}\text{Ru})_{\odot} = 2.97$ (Lodders 2003) for the solar system crucially depends on other sources for these isotopes. In this regard, although both these ratios can be achieved in the wind (see Figs. 4–6), this result is largely irrelevant for explaining the relative abundances of $^{92,94}\text{Mo}$ ($^{96,98}\text{Ru}$) in the solar system.

For illustration, we show in Fig. 7 models based on the trajectory ejected at $t_{\text{pb}} = 8$ s that produce $^{92,94}\text{Mo}$ ($^{96,98}\text{Ru}$) in the solar ratio but have little to do with accounting for their abundance ratio in the solar system.

The solar ratio for $^{92,94}\text{Mo}$ can be achieved in neutron-rich winds for $S = 60$ k_{B}/nuc and $Y_e(0) = 0.475$ (top panel) or in proton-rich winds for $S = 120$ k_{B}/nuc and $Y_e(0) = 0.58$ (middle panel). However, in neutron-rich winds, the predominantly produced isotopes are ^{88}Sr , ^{89}Y , and ^{90}Zr with the magic neutron number $N = 50$ (Hoffman et al. 1997, 1996; Wittl et al. 1994), while the production factors for $^{92,94}\text{Mo}$ are only $\approx 2 \times 10^{-3} P_{\text{max}}$. These production factors dramatically increase to $\approx 0.1 P_{\text{max}}$ for proton-rich winds, but in this case ^{98}Ru has the largest production factor and ^{96}Ru is coproduced in a non-solar ratio. Nevertheless, this case represents approximately the optimal scenario for wind contributions to the solar abundances of $^{92,94}\text{Mo}$ and $^{96,98}\text{Ru}$. Finally, the solar ratio for $^{96,98}\text{Ru}$ can be achieved in proton-rich winds for $S = 60$ k_{B}/nuc and $Y_e(0) = 0.59$ (bottom panel). However, for these conditions the predominantly produced isotopes are ^{74}Se , ^{78}Kr , and ^{84}Sr .

Fisker et al. (2009) found that $^{92,94}\text{Mo}$ could be produced in the solar ratio in slightly proton-rich winds but with too small production factors to account for their solar abundances. Those results are qualitatively consistent with ours, although Fisker et al. (2009) used very different trajectories.

3.2. Peculiar Mo patterns in SiC X grains

Relative to ^{96}Mo , an s -only isotope, the p -only isotopes $^{92,94}\text{Mo}$ and the r -only isotope ^{100}Mo are nearly absent in mainstream SiC grains. This points to an s -process origin in AGB stars for the Mo patterns in such grains (see e.g., Lugaro et al. 2003 for a detailed study). In contrast, SiC X grains have peculiar Mo patterns with large enrichments in the mixed isotopes $^{95,97}\text{Mo}$ (Pellin et al. 1999, 2006). Some of the X grains are also highly enriched in the r -only isotope ^{96}Zr (Davis et al. 1999; Pellin et al. 2006). While an r -process origin may possibly account for the large enrichments in ^{96}Zr and $^{95,97}\text{Mo}$, this is inconsistent with the data on the r -only isotope ^{100}Mo , which is not significantly enriched in most SiC X grains (Pellin et al. 1999, 2006).

Meyer et al. (2000) proposed to explain the overabundance of $^{95,97}\text{Mo}$ in SiC X grains with a neutron burst model (Howard et al. 1992). They first exposed a solar distribution of nuclei to a weak neutron fluence to mimic the weak s -process during the presupernova phase of a massive star (see e.g., Pignatari et al. 2010; Käppeler et al. 2011). Then they abruptly heated the processed matter to 1 GK to mimic the effect of a supernova shock and allowed the shocked matter to expand and cool. The burst of neutrons released by (α, n) reactions redistributed the initial abundances of Y and Zr isotopes to heavier isotopes up to $A \sim 97$, but the burst was not strong enough to accumulate much matter at ^{100}Zr . The original abundances of Mo isotopes were also redistributed to heavier isotopes. Finally, large abundances of $^{95,97}\text{Mo}$ were obtained upon the β decay of ^{95}Y and $^{95,97}\text{Zr}$ that were newly synthesized by the neutron burst.

While the above neutron burst model offers a potential explanation of the enrichments in ^{96}Zr and $^{95,97}\text{Mo}$ in SiC X grains, it remains to be seen if the conditions assumed could be provided by a detailed astrophysical model. Here we explore another potential explanation based on the neutrino-driven wind. Figure 8 shows the produc-

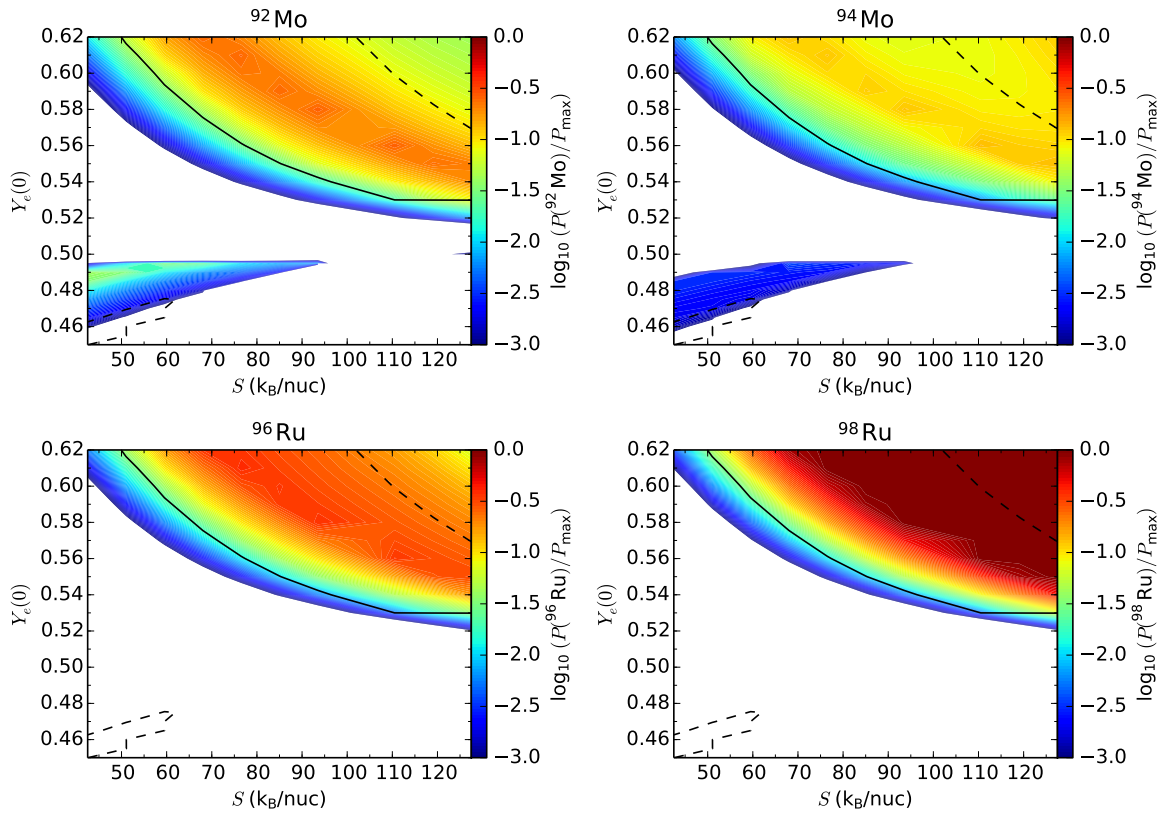


FIG. 4.— Color-coded contours illustrate the ratios (on a logarithmic scale) of the production factors of $^{92,94}\text{Mo}$ (upper panels) and $^{96,98}\text{Ru}$ (lower panels) relative to the maximum production factor among all isotopes produced by the trajectory ejected at $t_{\text{pb}} = 8$ s for different $Y_e(0)$ and S . Ratios smaller than 10^{-3} are shown in white. For reference, the solid (dashed) curves correspond to conditions where the ratio $X(^{96}\text{Ru})/X(^{98}\text{Ru})$ [$X(^{92}\text{Mo})/X(^{94}\text{Mo})$] produced by the trajectory reaches the solar system value with the abundances of $^{96,98}\text{Ru}$ ($^{92,94}\text{Mo}$) exceeding 10^{-10} .

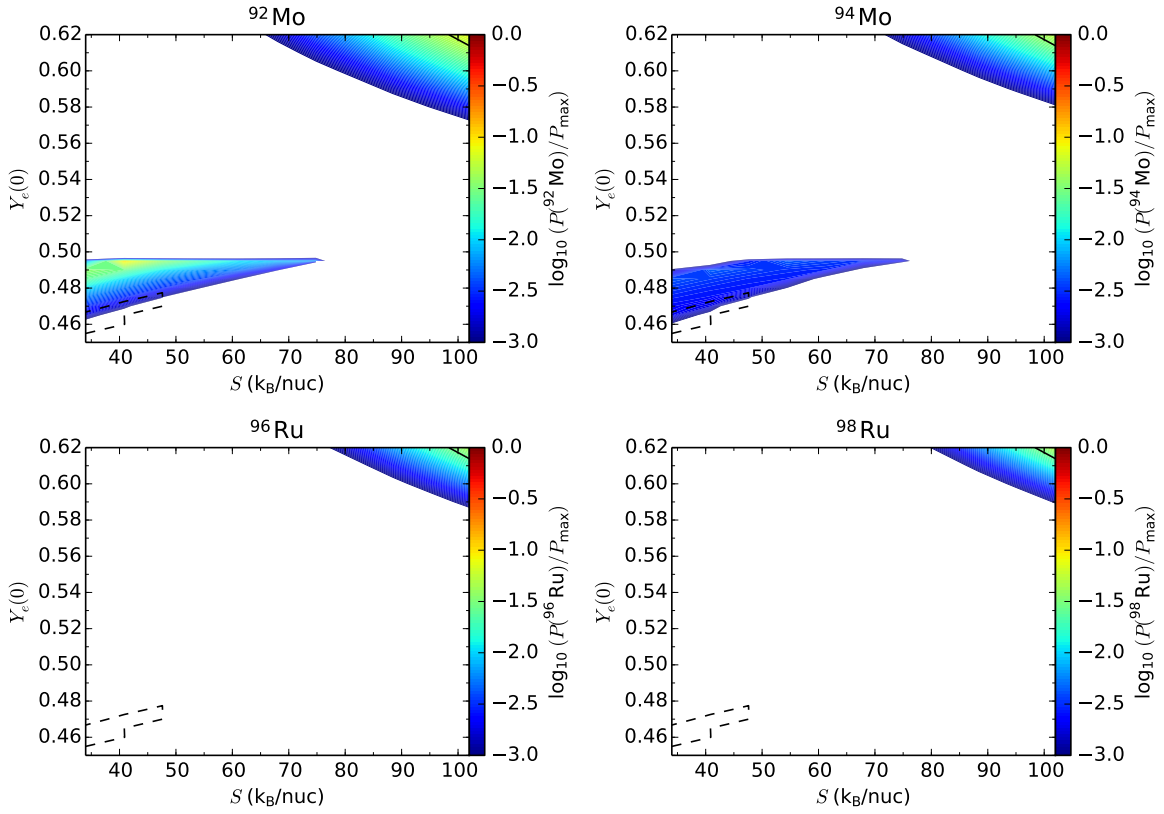


FIG. 5.— Same as Fig. 4, but for the trajectory ejected at $t_{\text{pb}} = 2$ s.

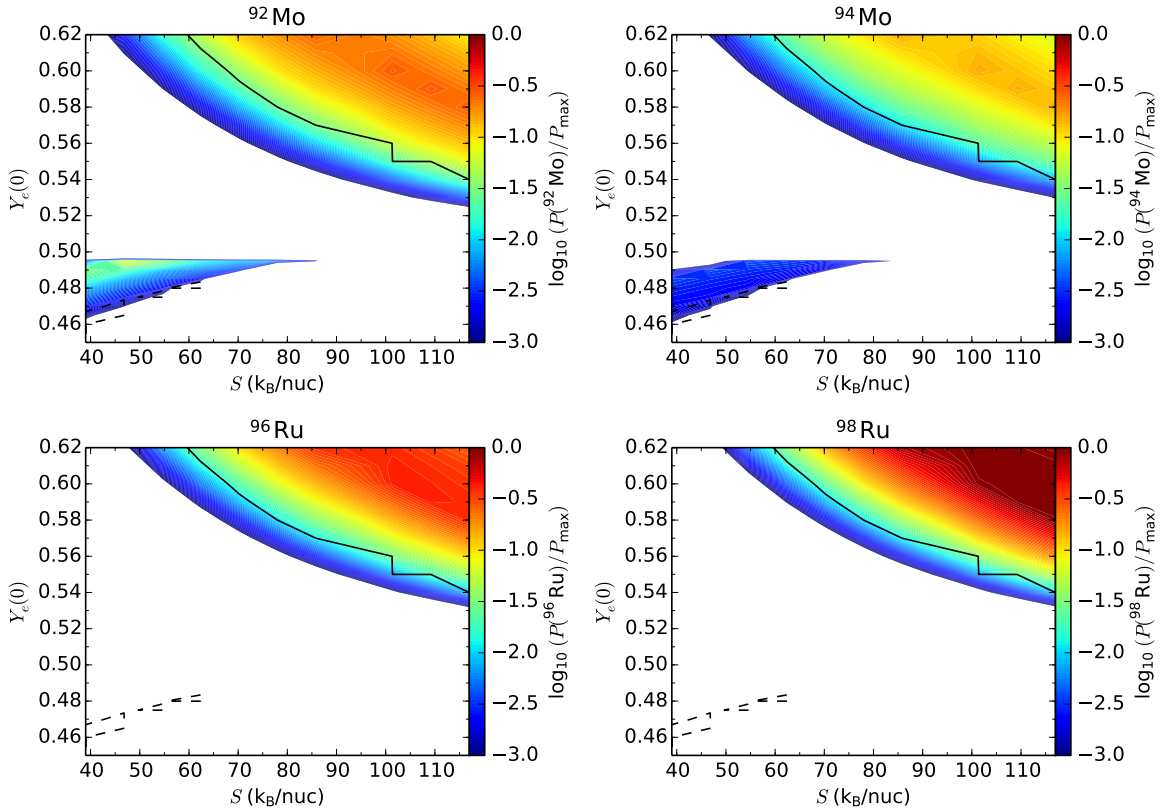


FIG. 6.— Same as Fig. 4, but for the trajectory ejected at $t_{\text{pb}} = 5$ s.

tion factors for various isotopes made in the wind that

corresponds to the trajectory ejected at $t_{\text{pb}} = 8$ s with

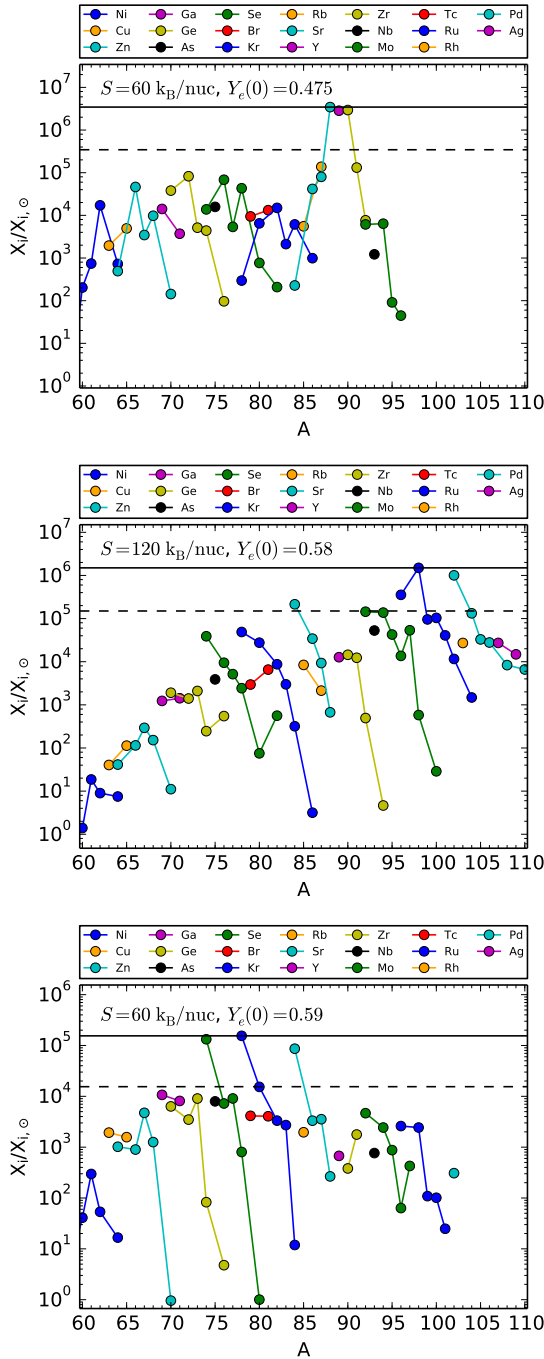


FIG. 7.— The ratio of the mass fraction of an isotope produced by the wind trajectory ejected at $t_{\text{pb}} = 8$ s (X_i) relative to that observed in the solar system ($X_{i,\odot}$), i.e., the production factor, as a function of the mass number (A). Isotopes from the same element are connected by line segments. The horizontal lines indicate a normalization band given by the largest production factor (solid line) and a factor 10 less (dashed line). Nuclei falling within the band are the main products. The solar ratio of $^{92,94}\text{Mo}$ is achieved in the top and middle panels, while that of $^{96,98}\text{Ru}$ is achieved in the bottom panel. However, the actual ratio of $^{92,94}\text{Mo}$ in the solar system must be explained mostly by sources other than the wind, and that of $^{96,98}\text{Ru}$ by combining the wind and other sources.

$S = 110$ k_{B}/nuc and $Y_e(0) = 0.47$. It can be seen that ^{96}Zr has the largest production factor and $^{95,97,98,100}\text{Mo}$ are also significantly produced. Further, the production factors for $^{95,97}\text{Mo}$ exceed those for $^{98,100}\text{Mo}$, in agree-

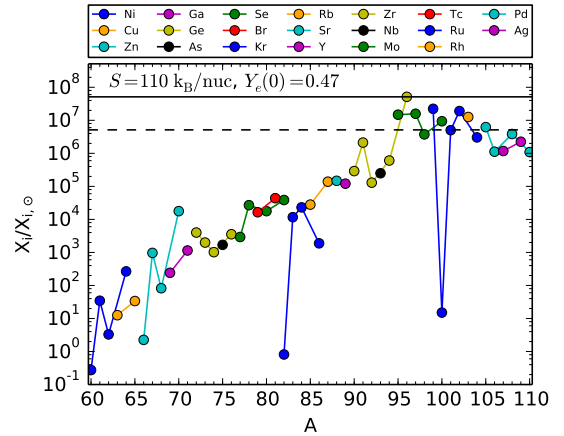


FIG. 8.— Same as Fig. 7, but for wind conditions that are relevant for explaining the peculiar patterns of $^{95,97,98,100}\text{Mo}$ found in SiC X grains.

ment with the patterns in SiC X grains (Pellin et al. 1999, 2006). Specifically, the ratios of the production factors are $P(^{95}\text{Mo}) : P(^{97}\text{Mo}) : P(^{98}\text{Mo}) : P(^{100}\text{Mo}) = 1.5 : 1.64 : 0.393 : 1$. Note also that neither the p -only isotopes $^{92,94}\text{Mo}$ nor the s -only isotope ^{96}Mo is produced in this wind.

Because the sources for $^{92,94}\text{Mo}$ are uncertain, we focus on explaining the patterns of $^{95,96,97,98,100}\text{Mo}$ in SiC X grains. We consider that these five isotopes can be accounted for by mixtures of contributions from the s -process, the r -process, and the neutrino-driven wind. Specifically, we assign the s -only isotope ^{96}Mo exclusively to the s -process and use its abundance in a grain along with the solar s -process pattern to determine the s -process contributions to other Mo isotopes. Because the “ r -only” isotope ^{100}Mo cannot be made in the s -process, we assign a fraction f_w of its abundance in a grain to the wind and the rest to the r -process. The r -process fraction $(1 - f_w)$ of the ^{100}Mo abundance in a grain is used along with the solar r -process pattern to determine the r -process contributions to other Mo isotopes. Consequently, the abundance of the isotope ^iMo in a grain, $(^i\text{Mo})_g$, is given by

$$(^i\text{Mo})_g = \left(\frac{^i\text{Mo}}{^{96}\text{Mo}} \right)_s (^{96}\text{Mo})_g + \left[(1 - f_w) \left(\frac{^i\text{Mo}}{^{100}\text{Mo}} \right)_r + f_w \left(\frac{^i\text{Mo}}{^{100}\text{Mo}} \right)_w \right] (^{100}\text{Mo})_g, \quad (2)$$

where the s -process, r -process, and wind production ratios $(^i\text{Mo}/^{96}\text{Mo})_s$, $(^i\text{Mo}/^{100}\text{Mo})_r$, and $(^i\text{Mo}/^{100}\text{Mo})_w$ are assumed to be fixed.

Equation (2) can be rewritten as

$$\frac{(^i\text{Mo}/^{96}\text{Mo})_g}{(^i\text{Mo}/^{96}\text{Mo})_{\odot}} = f_{s,\odot} (^i\text{Mo}) + \left[(1 - f_w) f_{r,\odot} (^i\text{Mo}) + f_w \frac{P(^i\text{Mo})}{P(^{100}\text{Mo})} \right] \frac{(^{100}\text{Mo}/^{96}\text{Mo})_g}{(^{100}\text{Mo}/^{96}\text{Mo})_{\odot}}, \quad (3)$$

where $f_{s,\odot} (^i\text{Mo})$ and $f_{r,\odot} (^i\text{Mo}) = 1 - f_{s,\odot} (^i\text{Mo})$ are the s -process and r -process fractions of the solar ^iMo abundance, respectively. We take $f_{s,\odot} (^i\text{Mo}) = 0.50, 0.59, 0.75, \text{ and } 0$ for $^{95}\text{Mo}, ^{97}\text{Mo}, ^{98}\text{Mo}, \text{ and } ^{100}\text{Mo}$, respec-

tively. These values are consistent with both the estimates of Arlandini et al. (1999) and the s -process patterns found in mainstream SiC grains (e.g., Pellin et al. 1999). Note that $f_{r,\odot}(^i\text{Mo}) = 1 - f_{s,\odot}(^i\text{Mo})$ is valid when the wind makes negligible contributions to the solar abundances of the relevant Mo isotopes.

In terms of the meteoritic notation

$$\delta ^i\text{Mo} \equiv 1000 \times \left[\frac{(^i\text{Mo}/^{96}\text{Mo})_g}{(^i\text{Mo}/^{96}\text{Mo})_\odot} - 1 \right], \quad (4)$$

Eq. (3) can be written as

$$\delta ^i\text{Mo} = 10^3 f_w \left[\frac{P(^i\text{Mo})}{P(^{100}\text{Mo})} - f_{r,\odot}(^i\text{Mo}) \right] + \left[(1 - f_w) f_{r,\odot}(^i\text{Mo}) + f_w \frac{P(^i\text{Mo})}{P(^{100}\text{Mo})} \right] \delta ^{100}\text{Mo}. \quad (5)$$

Using the central value of $\delta ^{100}\text{Mo}$ for a grain along with the wind production factor $P(^i\text{Mo})$ relative to $P(^{100}\text{Mo})$ and the solar r -process fraction $f_{r,\odot}(^i\text{Mo})$ given above, we find f_w for which Eq. (5) gives $\delta ^i\text{Mo}$ in good agreement with the data on $^{95,97,98}\text{Mo}$ in the same grain. These results are shown in Fig. 9 with $f_w = 0.23, 0.3, 0.7, 0.45,$ and 1 for five SiC X grains 113-2, 113-3, 209-1, 100-2, and B2-05 (Pellin et al. 2006), respectively. It can be seen that the above simple model including the wind contributions can explain the overall peculiar patterns of $^{95,97,98,100}\text{Mo}$ found in these grains. We expect that better agreement with the data, e.g., elimination of the discrepancy for ^{98}Mo in the grain 209-1, may be achieved by varying $\delta ^{100}\text{Mo}$ within the measurement errors or using different wind conditions to optimize the wind production factors, or both. However, we consider that the results shown in Fig. 9 are sufficient as a proof

of concept.

4. CONCLUSIONS

We have presented a detailed parametric study on the production of Mo and Ru isotopes in neutrino-driven winds. Our results can be generalized if conditions similar to those studied here are also obtained for other types of ejecta in either CCSNe or neutron star mergers. Consequently, our study is complementary to post-processing studies based on specific simulations of these events. With regard to the p -isotopes, we find that proton-rich winds can make dominant contributions to the solar abundance of ^{98}Ru , significant contributions to those of ^{96}Ru ($\lesssim 40\%$) and ^{92}Mo ($\lesssim 27\%$), and relatively minor contributions to that of ^{94}Mo ($\lesssim 14\%$). In contrast, neutron-rich winds make negligible contributions to the solar abundances of $^{92,94}\text{Mo}$ and cannot produce $^{96,98}\text{Ru}$. However, we have shown that some neutron-rich winds can account for the peculiar patterns of $^{95,97,98,100}\text{Mo}$ in SiC X grains.

In conclusion, our results strongly suggest that the solar abundances of $^{92,94}\text{Mo}$ are dominantly produced by sources other than the neutrino-driven wind. In addition, while the wind can be a dominant source for the ^{98}Ru in the solar system, other sources are also required to account for the ^{96}Ru .

This work was supported in part by the Helmholtz-University Young Investigator grant No. VH-NG-825, Deutsche Forschungsgemeinschaft through SFB 1245, BMBF under grant No. 05P15RDFN1, ERC 677912 EUROPIUM, and the US DOE grant DE-FG02-87ER40328. We acknowledge useful discussions with Camilla J. Hansen, Maria Lugaro, Marco Pignatari, and Claudia Travaglio.

REFERENCES

- Angulo, C., Arnould, M., Rayet, M., Descouvemont, P., Baye, D., Leclercq-Willain, C., Coc, A., Barhoumi, S., Aguer, P., Rolfs, C., Kunz, R., Hammer, J. W., Mayer, A., Paradellis, T., Kossionides, S., Chronidou, C., Spyrou, K., degl'Innocenti, S., Fiorentini, G., Ricci, B., Zavatarelli, S., Providencia, C., Wolters, H., Soares, J., Grama, C., Rahighi, J., Shoter, A., & Laméhi Rachtı, M. 1999, *Nuclear Physics A*, 656, 3
- Arcones, A. & Bliss, J. 2014, *J. Phys. G: Nucl. Phys.*, 41, 044005
- Arcones, A., Fröhlich, C., & Martínez-Pinedo, G. 2012, *ApJ*, 750, 18
- Arcones, A. & Janka, H.-T. 2011, *A&A*, 526, A160+
- Arcones, A., Janka, H.-T., & Scheck, L. 2007, *A&A*, 467, 1227
- Arcones, A. & Montes, F. 2011, *ApJ*, 731, 5
- Arcones, A. & Thielemann, F.-K. 2013, *J. Phys. G: Nucl. Phys.*, 40, 013201
- Arlandini, C., Käppeler, F., Wisshak, K., Gallino, R., Lugaro, M., Busso, M., & Straniero, O. 1999, *ApJ*, 525, 886
- Arnould, M. & Goriely, S. 2003, *Phys. Rep.*, 384, 1
- Banerjee, P., Haxton, W. C., & Qian, Y.-Z. 2011, *Physical Review Letters*, 106, 201104
- Bliss, J., Arcones, A., Montes, F., & Pereira, J. 2017, *J. Phys. G: Nucl. Phys.*, 44, 054003
- Bliss, J., Witt, M., Arcones, A., Montes, F., & Pereira, J. 2018, *ApJ*, 855, 135
- Burbidge, E. M., Burbidge, G. R., Fowler, W. A., & Hoyle, F. 1957, *Rev. Mod. Phys.*, 29, 547
- Cameron, A. G. W. 1957, *AJ*, 62, 9
- Davis, A. M., Pellin, M. J., Lewis, R. S., Amari, S., & Clayton, R. N. 1999, *Meteoritics & Planet. Sci. Suppl.*, 34, 30
- Farouqi, K., Kratz, K.-L., Mashonkina, L. I., Pfeiffer, B., Cowan, J. J., Thielemann, F.-K., & Truran, J. W. 2009, *ApJ*, 694, L49
- Fisker, J. L., Hoffman, R. D., & Pruet, J. 2009, *ApJ*, 690, L135
- Freiburghaus, C., Rembges, J.-F., Rauscher, T., Kolbe, E., Thielemann, F.-K., Kratz, K.-L., Pfeiffer, B., & Cowan, J. J. 1999a, *ApJ*, 516, 381
- Freiburghaus, C., Rosswog, S., & Thielemann, F.-K. 1999b, *ApJ*, 525, L121
- Fröhlich, C., Martínez-Pinedo, G., Liebendörfer, M., Thielemann, F.-K., Bravo, E., Hix, W. R., Langanke, K., & Zinner, N. T. 2006, *Phys. Rev. Lett.*, 96, 142502
- Goriely, S., Bauswein, A., & Janka, H.-T. 2011, *ApJ*, 738, L32
- Hansen, C. J., Montes, F., & Arcones, A. 2014, *ApJ*, 797, 123
- Hoffman, R. D., Woosley, S. E., Fuller, G. M., & Meyer, B. S. 1996, *ApJ*, 460, 478
- Hoffman, R. D., Woosley, S. E., & Qian, Y.-Z. 1997, *ApJ*, 482, 951
- Howard, W. M., Meyer, B. S., & Clayton, D. D. 1992, *Meteoritics*, 27, 404
- Janka, H.-T. 2012, *Ann. Rev. Nucl. Part. Sc.*, 62, 407
- Käppeler, F., Gallino, R., Bisterzo, S., & Aoki, W. 2011, *Rev. Mod. Phys.*, 83, 157
- Kasen, D., Metzger, B., Barnes, J., Quataert, E., & Ramirez-Ruiz, E. 2017, *Nature*, 551, 80
- Korobkin, O., Rosswog, S., Arcones, A., & Winteler, C. 2012, *MNRAS*, 426, 1940
- Lodders, K. 2003, *ApJ*, 591, 1220
- Lugaro, M., Davis, A. M., Gallino, R., Pellin, M. J., Straniero, O., & Käppeler, F. 2003, *ApJ*, 593, 486
- Meyer, B. S. 1994, *ARA&A*, 32, 153
- Meyer, B. S. & Brown, J. S. 1997, *ApJS*, 112, 199
- Meyer, B. S., Clayton, D. D., & The, L.-S. 2000, *ApJ*, 540, L49

- Nishimura, N., Takiwaki, T., & Thielemann, F.-K. 2015, *ApJ*, 810, 109
- NuDat2. 2013, National Nuclear Data Center, information extracted from the NuDat 2 database, <http://www.nndc.bnl.gov/nudat2/>
- Otsuki, K., Tagoshi, H., Kajino, T., & Wanajo, S. 2000, *ApJ*, 533, 424
- Pellin, M. J., Davis, A. M., Lewis, R. S., Amari, S., & Clayton, R. N. 1999, in *Lunar & Planet. Sci. Conf.*, Vol. 30, 1969
- Pellin, M. J., Savina, M. R., Calaway, W. F., Tripa, C. E., Barzyk, J. G., Davis, A. M., Gyngard, F., Amari, S., Zinner, E., Lewis, R. S., & Clayton, R. N. 2006, in *Lunar & Planet. Sci. Conf.*, Vol. 37, 2041
- Pignatari, M., Gallino, R., Heil, M., Wiescher, M., Käppeler, F., Herwig, F., & Bisterzo, S. 2010, *ApJ*, 710, 1557
- Pignatari, M., Göbel, K., Reifarth, R., & Travaglio, C. 2016, *International Journal of Modern Physics E*, 25, 1630003
- Pruet, J., Hoffman, R. D., Woosley, S. E., Janka, H.-T., & Buras, R. 2006, *ApJ*, 644, 1028
- Qian, Y.-Z. 2014, *Journal of Physics G Nuclear Physics*, 41, 044002
- Qian, Y.-Z. & Wasserburg, G. J. 2007, *Phys. Rep.*, 442, 237
- Qian, Y.-Z. & Woosley, S. E. 1996, *ApJ*, 471, 331
- Raiteri, C. M., Gallino, R., Busso, M., Neuberger, D., & Käppeler, F. 1993, *ApJ*, 419, 207
- Rauscher, T. & Thielemann, F.-K. 2000, *At. Data Nucl. Data Tables*, 75, 1
- Reaclib. 2013, Database of Joint Institute of Nuclear Astrophysics, <http://www.jinaweb.org>
- Smartt, S. J., Chen, T.-W., Jerkstrand, A., Coughlin, M., Kankare, E., Sim, S. A., Fraser, M., Inserra, C., Maguire, K., Chambers, K. C., Huber, M. E., Krühler, T., Leloudas, G., Magee, M., Shingles, L. J., Smith, K. W., Young, D. R., Tonry, J., Kotak, R., Gal-Yam, A., Lyman, J. D., Homan, D. S., Agliozzo, C., Anderson, J. P., Angus, C. R., Ashall, C., Barbarino, C., Bauer, F. E., Berton, M., Botticella, M. T., Bulla, M., Bulger, J., Cannizzaro, G., Cano, Z., Cartier, R., Cikota, A., Clark, P., De Cia, A., Della Valle, M., Denneau, L., Dennefeld, M., Dessart, L., Dimitriadis, G., Elias-Rosa, N., Firth, R. E., Flewelling, H., Flörs, A., Franckowiak, A., Frohmaier, C., Galbany, L., González-Gaitán, S., Greiner, J., Gromadzki, M., Guelbenzu, A. N., Gutiérrez, C. P., Hamanowicz, A., Hanlon, L., Harmanen, J., Heintz, K. E., Heinze, A., Hernandez, M.-S., Hodgkin, S. T., Hook, I. M., Izzo, L., James, P. A., Jonker, P. G., Kerzendorf, W. E., Klose, S., Kostrzewa-Rutkowska, Z., Kowalski, M., Kromer, M., Kuncarayakti, H., Lawrence, A., Lowe, T. B., Magnier, E. A., Manulis, I., Martin-Carrillo, A., Mattila, S., McBrien, O., Müller, A., Nordin, J., O'Neill, D., Onori, F., Palmerio, J. T., Pastorello, A., Patat, F., Pignata, G., Podsiadlowski, P., Pumo, M. L., Prentice, S. J., Rau, A., Razza, A., Rest, A., Reynolds, T., Roy, R., Rüter, A. J., Rybicki, K. A., Salmon, L., Schady, P., Schultz, A. S. B., Schweyer, T., Seitzzahl, I. R., Smith, M., Sollerman, J., Stalder, B., Stubbs, C. W., Sullivan, M., Szegedi, H., Taddia, F., Taubenberger, S., Terreran, G., van Soelen, B., Vos, J., Wainscoat, R. J., Walton, N. A., Waters, C., Weiland, H., Willman, M., Wiseman, P., Wright, D. E., Wyrzykowski, L., & Yaron, O. 2017, *Nature*, 551, 75
- Thompson, T. A., Burrows, A., & Meyer, B. S. 2001, *ApJ*, 562, 887
- Travaglio, C., Gallino, R., Rauscher, T., Dauphas, N., Röpke, F. K., & Hillebrandt, W. 2014, *ApJ*, 795, 141
- Wanajo, S. 2006, *ApJ*, 647, 1323
- Wanajo, S., Janka, H.-T., & Kubono, S. 2011, *ApJ*, 729, 46
- Witti, J., Janka, H.-T., & Takahashi, K. 1994, *A&A*, 286, 841
- Woosley, S. E. & Hoffman, R. D. 1992, *ApJ*, 395, 202

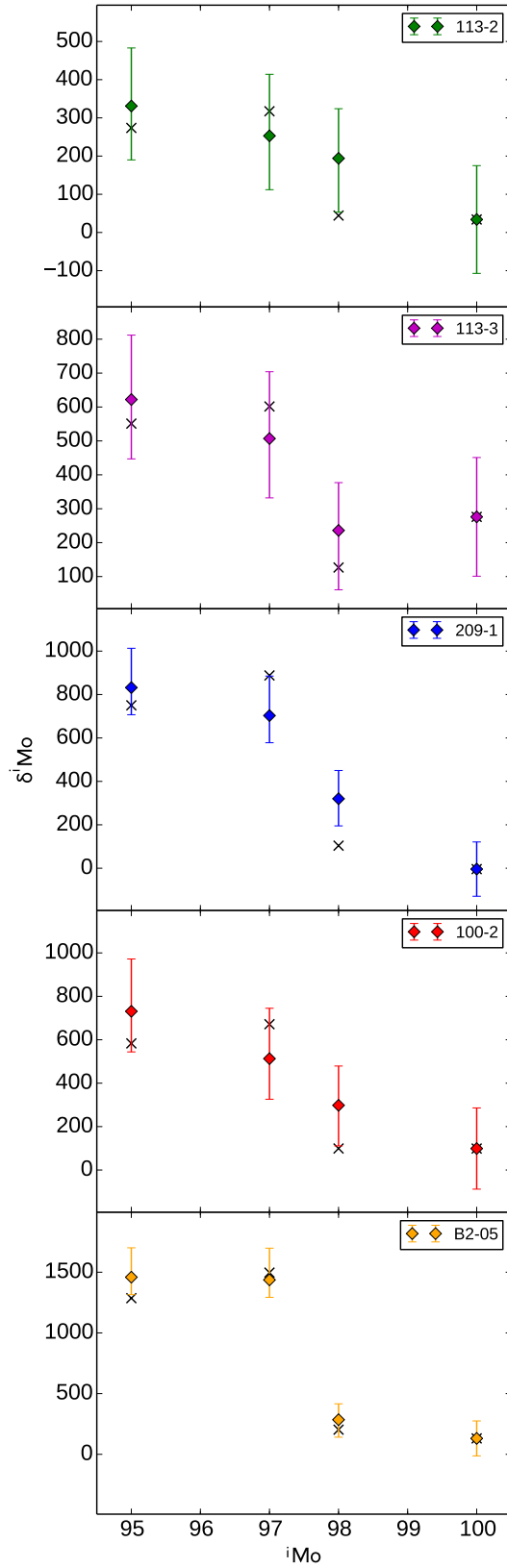


FIG. 9.— Comparison of the model (crosses) including wind contributions and the data (colored diamonds with error bars) on the peculiar patterns of $^{95,97,98,100}\text{Mo}$ in five SiC X grains (Pellin et al. 2006).